

THE EFFECTS OF RAM-PRESSURE STRIPPING AND SUPERNOVA WINDS ON THE TIDAL STIRRING OF DISKY DWARFS: ENHANCED TRANSFORMATION INTO DWARF SPHEROIDALS

STELIOS KAZANTZIDIS¹, LUCIO MAYER², SIMONE CALLEGARI³,
MASSIMO DOTTI⁴, AND LEONIDAS A. MOUSTAKAS⁵

Accepted by ApJL on January 21, 2017

ABSTRACT

A conclusive model for the formation of dwarf spheroidal (dSph) galaxies still remains elusive. Owing to their proximity to the massive spirals Milky Way (MW) and M31, various environmental processes have been invoked to explain their origin. In this context, the tidal stirring model postulates that interactions with MW-sized hosts can transform rotationally supported dwarfs, resembling present-day dwarf irregular (dIrr) galaxies, into systems with the kinematic and structural properties of dSphs. Using N -body+SPH simulations, we investigate the dependence of this transformation mechanism on the gas fraction, f_{gas} , in the disk of the progenitor dwarf. Our numerical experiments incorporate for the first time the combined effects of radiative cooling, ram-pressure stripping, star formation, supernova (SN) winds, and a cosmic UV background. For a given orbit inside the primary galaxy, rotationally supported dwarfs with gas fractions akin to those of observed dIrrs ($f_{\text{gas}} \gtrsim 0.5$), demonstrate a substantially enhanced likelihood and efficiency of transformation into dSphs relative to their collisionless ($f_{\text{gas}} = 0$) counterparts. We argue that the combination of ram-pressure stripping and SN winds causes the gas-rich dwarfs to respond more impulsively to tides, augmenting their transformation. When $f_{\text{gas}} \gtrsim 0.5$, disky dwarfs on previously unfavorable low-eccentricity or large-pericenter orbits are still able to transform. On the widest orbits, the transformation is incomplete; the dwarfs retain significant rotational support, a relatively flat shape, and some gas, naturally resembling transition-type systems. We conclude that tidal stirring constitutes a prevalent evolutionary mechanism for shaping the structure of dwarf galaxies within the currently favored CDM cosmological paradigm.

Subject headings: galaxies: dwarf – galaxies: formation – galaxies: kinematics and dynamics – galaxies: structure – Local Group – methods: numerical

1. INTRODUCTION

The Local Group (LG) and its population of dwarf spheroidal (dSph) galaxies provide crucial insights into cosmic structure formation. These extraordinary objects are the faintest and most dark matter (DM) dominated galaxies known (e.g., Mateo 1998; McConnachie 2012). Furthermore, dSphs are gas poor or completely devoid of gas (e.g., Grcevich & Putman 2009) and they are characterized by pressure-supported, spheroidal stellar components (e.g., Mateo 1998) and widely diverse star formation (SF) histories (e.g., Skillman et al. 2016).

Given that dSphs are preferentially located near the massive spirals Milky Way (MW) and M31, various environmental mechanisms have been invoked to explain their origin (e.g., Einasto et al. 1974; Faber & Lin 1983; Kroupa 1997; Mayer et al. 2001b,a, 2006, 2007; Kravtsov et al. 2004; D’Onghia et al. 2009; Klimentowski et al. 2009; Kazantzidis et al. 2011, 2013;

Pawlowski et al. 2011; Yozin & Bekki 2012)⁶. In this context, the “tidal stirring” model (Mayer et al. 2001b) posits that gravitational and hydrodynamical interactions with MW-sized hosts can transform rotationally supported dwarfs, resembling present-day dwarf irregulars (dIrrs), into systems with the kinematic and structural properties of dSphs.

Our study expands upon all previous investigations of tidal stirring in one major respect; the inclusion, for the first time, of the combined effects of ram-pressure stripping and supernova (SN) winds driving gas bulk motions and outflows. Such winds can directly affect the mass distribution of dwarf galaxies, significantly decreasing their total central density (e.g., Governato et al. 2010; Teyssier et al. 2013; Shen et al. 2014; Oñorbe et al. 2015; Read et al. 2016). In fact, any physical process (e.g., ram-pressure stripping) that can cause the removal of gas in dwarfs may reduce the inner density of their DM halos (e.g., Navarro et al. 1996a; Read & Gilmore 2005; Arraki et al. 2014).

This improvement in the modeling may be vital to tidal stirring. Indeed, systems with lower central densities are characterized by longer internal dynamical times and are thus expected to respond more impulsively to external tidal perturbations and suffer stronger tidal shocks (e.g., Gnedin & Ostriker 1999). Therefore, rotationally supported dwarfs with decreased central densities due

¹ Section of Astrophysics, Astronomy and Mechanics, Department of Physics, National and Kapodistrian University of Athens, 15784 Zografos, Athens, Greece; skazantzidis@phys.uoa.gr

² Center for Theoretical Astrophysics and Cosmology, Institute for Computational Science, University of Zürich, CH-8057 Zürich, Switzerland

³ Anthropology Institute and Museum, University of Zürich, CH-8057 Zürich, Switzerland

⁴ Università degli Studi di Milano-Bicocca, Piazza della Scienza 3, I-20126 Milano, Italy

⁵ Jet Propulsion Laboratory, California Institute of Technology, Pasadena, CA 91109, USA

⁶ For alternative scenarios of dSph formation, see, e.g., Sawala et al. (2010) and Assmann et al. (2013).

to baryonic effects may experience increasingly probable and efficient transformations into dSphs.

Here we explore this qualitative expectation via a series of tidal stirring simulations of disk dwarf galaxies with varying fractions of their disk mass in gas. Our results indicate that the likelihood and efficiency of transformation into a dSph are both enhanced significantly when the progenitor rotationally-supported dwarfs are gas-rich, with gas fractions that are in accordance with those inferred from observations and recent theoretical efforts in dwarf galaxy formation. This finding further establishes tidal stirring as a prevalent evolutionary mechanism for shaping the structure of dwarf galaxies within the currently favored CDM cosmological paradigm.

2. METHODS

We employed the technique of [Widrow et al. \(2008\)](#) to create self-consistent N-body realizations of rotationally supported dwarf galaxies consisting of exponential, baryonic disks embedded in cuspy, cosmologically-motivated [Navarro et al. \(1996b\)](#) DM halos.

Our goal is to elucidate the degree to which dSph formation via tidal stirring is affected by the presence of a gaseous component in the disk of the progenitor rotationally supported dwarf. To accomplish this, we varied the fraction of the disk mass in gas, f_{gas} , in three otherwise identically initialized disk dwarf galaxies; $f_{\text{gas}} = 0$, $f_{\text{gas}} = 0.5$, and $f_{\text{gas}} = 0.8$. The adopted values of $f_{\text{gas}} = 0.5$ are well-motivated as they are akin to those of both observed dIrrs (e.g., [McConnachie 2012](#); [Oh et al. 2015](#)) and simulated, realistic dIrr-like systems (e.g., [Governato et al. 2010](#); [Shen et al. 2014](#)).

Following [Widrow et al. \(2008\)](#), we first generated the dwarf model with a purely stellar disk ($f_{\text{gas}} = 0$). Subsequently, we converted a fraction f_{gas} of randomly selected stellar particles in the dwarf disk into gas particles, without changing their positions and masses [Dotti et al. \(2007\)](#). Gas particles were set on tangential orbits, with the dynamical equilibrium achieved by enforcing vertical pressure support to the disk, and by correcting their tangential velocities for the radial component of the pressure gradient force.

Each dwarf comprised a DM halo with a virial mass of $M_{\text{vir}} = 10^{10} M_{\odot}$, a choice that is motivated by theoretical studies of the mass distribution of satellites that could correspond to present-day dSphs (e.g., [Kravtsov et al. 2004](#); [Klimontowski et al. 2010](#); [Tomozeiu et al. 2016](#)). Informed by the same investigations, we constructed our dwarfs considering a $z = 1$ infall redshift onto the primary. The virial radius and the median concentration value for a $z = 1$ cosmological halo at this mass scale are $r_{\text{vir}} \approx 32.9$ kpc and $c \approx 9.4$, respectively (e.g., [Macciò et al. 2007](#)).

All dwarf galaxies hosted an identical, exponential baryonic disk whose mass, sech^2 vertical scale-height, and central radial velocity dispersion were $M_d = 0.02 M_{\text{vir}}$, $z_d = 0.2 R_d$, and $\sigma_{R0} = 15 \text{ km s}^{-1}$, respectively ([Kazantzidis et al. 2011](#)). Assuming a dimensionless halo spin parameter of $\lambda = 0.04$ yields a disk radial scale-length of $R_d \approx 0.76$ kpc ([Mo et al. 1998](#)).

Numerical parameters (i.e., particle numbers and gravitational softening lengths) for each component of the dwarf models are listed in [Table 1](#). For a given component, resolution (mass and force) was constant. This is

necessary in order to perform a numerically robust comparison among different simulations. We checked the adequacy of our dwarf models by evolving them for several Gyr in isolation (using an adiabatic equation of state for the gas-rich dwarfs) and confirming that they retained their equilibrium configuration.

For simplicity, we assumed a single host represented by a self-gravitating, high-resolution MW model ([Kazantzidis et al. 2011](#)). To explore the effect of ram pressure, we included an extended, non-rotating halo of hot gas in hydrostatic equilibrium inside the primary galaxy ([Mastropietro et al. 2005](#)) and with properties consistent with MW observations ([Miller & Bregman 2013](#)). We modeled this component with 6.25×10^6 particles and employed a fairly large gravitational softening, $\epsilon = 2$ kpc, to minimize discreteness noise in the host potential. The mass ratio of the gas particles in the dwarfs and those in the hot gas halo was 1, preventing spurious enhancement of ram-pressure stripping ([Abadi et al. 1999](#)).

Given that the $f_{\text{gas}} = 0.8$ disk dwarf is characterized by the largest gas fraction, we use it as the basis for the comparison with the $f_{\text{gas}} = 0$ model. To this end, each of these dwarfs was placed on seven bound orbits (O1–O7) of varying sizes and eccentricities inside the primary galaxy. [Table 2](#) summarizes the adopted orbital parameters, which are motivated by theoretical studies of the orbital distributions of cosmological satellites in MW-sized hosts (e.g., [Diemand et al. 2007](#); [Klimontowski et al. 2010](#)).

For completeness, we performed 8 additional simulations, for a total of 22 experiments (S1–S22; [Table 3](#)). Specifically, to ascertain the relative effect of f_{gas} on dSph formation, we followed the evolution of dwarf model $f_{\text{gas}} = 0.5$ on orbits O1–O3 (S15–S17). Moreover, in an effort to investigate whether the cosmic epoch at which the disk dwarfs were accreted by their hosts could affect their transformation, we evolved model $f_{\text{gas}} = 0.8$ on orbits O1–O3, assuming a larger $z = 2$ infall redshift onto the primary (S18–S20). This is relevant as a stronger cosmic UV background is expected to augment ram-pressure stripping by enhancing gas heating and ionization. In the latter set of simulations, we only modified the time evolution of the intensity of the cosmic UV background to reflect a $z = 2$ accretion epoch. To avoid introducing an additional parameter, the internal structure of the disk dwarf was explicitly not altered in these cases. We note that in all experiments described above (S1–S20), the alignments between the internal angular momenta of the dwarfs, that of the primary disk, and that of the orbital angular momenta, were all *mildly* prograde and equal to 45° ([Kazantzidis et al. 2011](#)).

Lastly, we explored the importance of the initial inclination of the dwarf disk with respect to the orbital plane by placing model $f_{\text{gas}} = 0.8$ on orbit O1 and changing the default value from $i = 45^\circ$ to $i = 0^\circ$ and to $i = 90^\circ$ (S21–S22). These two configurations correspond to a perfectly edge-on and a perfectly face-on disk and bracket the range of possible amplitudes for the ram-pressure force.

3. SIMULATIONS

All simulations were performed with the parallel Tree+SPH code *GASOLINE* ([Wadsley et al. 2004](#)).

TABLE 1
NUMERICAL PARAMETERS OF DWARF MODELS

| Model | f_{gas} | N_{DM} | N_* | N_{gas} | ϵ_{DM} (pc) | ϵ_* (pc) | ϵ_{gas} (pc) |
|-------|------------------|-----------------|-----------------|--------------------|--------------------------------|----------------------|---------------------------------|
| D1 | 0 | 10^6 | 2×10^6 | ... | 100 | 15 | ... |
| D2 | 0.5 | 10^6 | 10^6 | 6.25×10^4 | 100 | 15 | 50 |
| D3 | 0.8 | 10^6 | 4×10^5 | 10^5 | 100 | 15 | 50 |

TABLE 2
ORBITAL PARAMETERS OF DISKY DWARFS

| Orbit | r_{apo} (kpc) | r_{peri} (kpc) | $r_{\text{apo}}/r_{\text{peri}}$ |
|-------|---------------------------|----------------------------|----------------------------------|
| O1 | 125 | 25 | 5 |
| O2 | 85 | 17 | 5 |
| O3 | 250 | 50 | 5 |
| O4 | 125 | 12.5 | 10 |
| O5 | 125 | 50 | 2.5 |
| O6 | 80 | 50 | 1.6 |
| O7 | 250 | 12.5 | 20 |

We included Compton cooling, atomic cooling, and metallicity-dependent radiative cooling at low temperatures (Mashchenko et al. 2006). A uniform, time-variable cosmic UV background, causing the photoionization and photoheating of the gas, was implemented using the Haardt & Madau (2012) model. We incorporated the effects of SF and SN feedback (“blastwave” scheme) according to Stinson et al. (2006). These recipes are characterized by several parameters, including the gas density threshold for SF, n_{SF} , and we adopted the relevant values from Governato et al. (2010). We emphasize that our high SF density threshold ($n_{\text{SF}} = 10 \text{ atoms cm}^{-3}$) enables the development of a realistic clumpy, inhomogeneous ISM, where SF and energy injection from SN explosions occur in a clustered fashion. As we demonstrate below, this has profound consequences on dSph formation via tidal stirring. Lastly, our gas mass resolution and the employed value of n_{SF} ensure that there is no artificial fragmentation (Bate & Burkert 1997).

4. RESULTS

The response of the rotationally supported dwarfs to the host galaxy tidal field is assessed through the evolution of their masses, kinematics, and shapes. These properties were always computed within 0.76 kpc, a radius that corresponds to the scale-length of the initial disk. Employing this well-defined, fixed scale allows us to overcome the complications related to determining tidal radii (e.g., Read et al. 2006) and aids the comparison among different experiments.

We used the parameters c/a and V_{rot}/σ_* to quantify the shapes and kinematics of the dwarf galaxies: c , a , V_{rot} , and σ_* correspond to the minor axis, the major axis, the rotational velocity, and the one-dimensional velocity dispersion of the stellar distribution, respectively. At each simulation output, we determined the directions of the principal axes and computed c/a via the moments of the inertia tensor. Subsequently, we calculated the rotational velocity around the minor axis, $V_{\text{rot}} = V_{\phi}$, and the dispersions σ_r , σ_{θ} , and σ_{ϕ} around the mean values; σ_* , which measures the amount of stellar random mo-

tions, is defined as $\sigma_* \equiv [(\sigma_r^2 + \sigma_{\theta}^2 + \sigma_{\phi}^2)/3]^{1/2}$.

Figure 1 shows the time evolution of the kinematics and shapes of the simulated disk dwarfs as they orbit inside the primary. In agreement with previous studies (e.g., Kazantzidis et al. 2011, 2013), the repeated action of the host galaxy tidal field causes simultaneously a progressive decrease of V_{rot}/σ_* and a continuous increase of c/a . Such evolution, which is strongly associated with pericentric passages where tidal shocks occur, designates the gradual transformation of the disk dwarfs into spheroidal stellar systems dominated by random motions.

Our goal is to determine the likelihood and efficiency of dSph formation via tidal stirring. To this end, we classify as bona fide dSphs only those simulated dwarfs whose final states are characterized by $V_{\text{rot}}/\sigma_* \lesssim 0.5$, $c/a \gtrsim 0.7$, and $M_{\text{gas}} \simeq 0$ (e.g., Mateo 1998; McConnachie 2012). We underscore that the criterion $V_{\text{rot}}/\sigma_* \lesssim 0.5$ is fairly conservative (Kazantzidis et al. 2013). Indeed, we measure V_{rot} around the minor axis of the stellar distribution, which corresponds to observing the simulated dwarfs perfectly edge-on. Adopting a random line-of-sight would result in smaller V_{rot}/σ_* values, indicating even more complete transformations.

Table 3 summarizes our results. During the orbital evolution of the dwarfs, the strong tidal forces at pericenters may trigger bar instabilities in their disks; column 6 refers to whether such a tidally induced bar was formed⁷. Columns 7–9 list the final values of M_{gas} , V_{rot}/σ_* and c/a , respectively. Column 10 specifies whether a dSph was produced according to our criteria. Column 11 reports the time elapsed from the beginning of the simulation until dSph formation occurs (the number of corresponding pericentric passages is included in parentheses).

Of the collisionless disk dwarfs, only those on high-eccentricity ($r_{\text{apo}}/r_{\text{peri}} \gtrsim 5$) and small-pericenter ($r_{\text{peri}} \lesssim 25 \text{ kpc}$) orbits that have also experienced at least three pericentric passages are transformed into dSphs. Interestingly, the likelihood and efficiency of dSph formation are both enhanced significantly for gas-rich ($f_{\text{gas}} \gtrsim 0.5$) dwarfs; in such cases, not only the transformation into a dSph occurs on previously unfavorable, low-eccentricity and/or large-pericenter orbits, but also the number of required pericentric passages for dSph formation is invariably smaller.

Figure 2 presents, in representative cases, the time evolution of both total and gas mass of the dwarfs and offers insight into these findings. In addition to illustrating the continuous decrease of the dwarf masses by the primary tidal field, this figure demonstrates that stripping of the total mass depends sensitively on f_{gas} . Indeed, while mass loss from the inner regions of the collisionless dwarf galaxies is relatively gentle and gradual, stripping is significantly boosted for gas-rich dwarfs. The strongest episodes of mass loss coincide with pericentric passages, where ram-pressure stripping is also maximal. At such times, the differences with the collisionless simulations are remarkable and become even more pronounced with higher gas fractions.

The rapid removal of gas via ram pressure, aided

⁷ Following Kazantzidis et al. (2011), we designate bar formation when the amplitude of the $m = 2$ Fourier component satisfies $A_2 \gtrsim 0.2$ between two consecutive pericentric passages.

TABLE 3
 SUMMARY OF RESULTS

| Simulation | f_{gas} | z | i (deg) | Orbit | Bar Formation | M_{gas} ($10^7 M_{\odot}$) | V_{rot}/σ_* | c/a | Classification | t_{dSph} (Gyr) |
|------------|------------------|-----|--------------|-------|------------------|--|---------------------------|-------|----------------|----------------------------|
| (1) | (2) | (3) | (4) | (5) | (6) | (7) | (8) | (9) | (10) | (11) |
| S1 | 0 | 1 | 45 | O1 | Yes | ... | 0.28 | 0.73 | dSph | 7.65 (5) |
| S2 | 0 | 1 | 45 | O2 | Yes | ... | 0.00 | 0.96 | dSph | 3.75 (4) |
| S3 | 0 | 1 | 45 | O3 | No | ... | 0.69 | 0.40 | Non-dSph | ... |
| S4 | 0 | 1 | 45 | O4 | Yes | ... | 0.01 | 0.97 | dSph | 4.00 (3) |
| S5 | 0 | 1 | 45 | O5 | No | ... | 0.80 | 0.50 | Non-dSph | ... |
| S6 | 0 | 1 | 45 | O6 | No | ... | 0.76 | 0.61 | Non-dSph | ... |
| S7 | 0 | 1 | 45 | O7 | Yes | ... | 0.39 | 0.54 | Non-dSph | ... |
| S8 | 0.8 | 1 | 45 | O1 | No | 0.00 | 0.12 | 0.95 | dSph | 3.55 (2) |
| S9 | 0.8 | 1 | 45 | O2 | No | 0.00 | 0.01 | 0.89 | dSph | 2.05 (2) |
| S10 | 0.8 | 1 | 45 | O3 | No | 2.34 | 0.89 | 0.62 | Non-dSph | ... |
| S11 | 0.8 | 1 | 45 | O4 | No | 0.00 | 0.03 | 0.90 | dSph | 2.70 (2) |
| S12 | 0.8 | 1 | 45 | O5 | No | 0.00 | 0.15 | 0.94 | dSph | 7.65 (4) |
| S13 | 0.8 | 1 | 45 | O6 | No | 0.00 | 0.12 | 0.94 | dSph | 5.80 (4) |
| S14 | 0.8 | 1 | 45 | O7 | No | 0.00 | 0.33 | 0.88 | dSph | 5.60 (2) |
| S15 | 0.5 | 1 | 45 | O1 | No | 0.00 | 0.02 | 0.96 | dSph | 4.05 (2) |
| S16 | 0.5 | 1 | 45 | O2 | No | 0.00 | 0.01 | 0.82 | dSph | 2.15 (2) |
| S17 | 0.5 | 1 | 45 | O3 | No | 1.04 | 1.05 | 0.53 | Non-dSph | ... |
| S18 | 0.8 | 2 | 45 | O1 | No | 0.00 | 0.10 | 0.92 | dSph | 3.55 (2) |
| S19 | 0.8 | 2 | 45 | O2 | No | 0.00 | 0.00 | 0.86 | dSph | 2.05 (2) |
| S20 | 0.8 | 2 | 45 | O3 | No | 0.97 | 0.75 | 0.75 | Non-dSph | ... |
| S21 | 0.8 | 1 | 0 | O1 | No | 0.00 | 0.08 | 0.93 | dSph | 3.65 (2) |
| S22 | 0.8 | 1 | 90 | O1 | No | 0.00 | 0.14 | 0.94 | dSph | 3.65 (2) |

by SN explosions, reduces swiftly the central densities of the gas-rich disk dwarfs. Therefore, these systems should respond more impulsively to tides and experience stronger tidal effects relative to their collisionless counterparts. Indeed, in the impulse approximation, tidal shocks lead to an energy increase given by $\Delta E/E \propto R^3/M$, where M corresponds to the total dwarf mass within a characteristic radius R (see Kazantzidis et al. 2011 for a detailed discussion). Owing to ram-pressure stripping, at a given distance R from the center of our dwarfs, increasing gas fractions correspond to smaller M , and thus to larger $\Delta E/E$; hence, the gas-rich dwarfs suffer more effective tidal shocks, which explains both their enhanced mass loss and augmented morphological transformation into dSph-like systems. Taking into account adiabatic corrections (e.g., Gnedin & Ostriker 1999) strengthens this conclusion. Indeed, for less concentrated mass distributions, adiabatic corrections result in even larger $\Delta E/E$ compared to those predicted by the impulse approximation.

Apart from amplifying ram-pressure stripping, SN winds play another crucial role in causing the gas-rich dwarfs to exhibit a more impulsive response to tides. This role is revealed in Figure 2, which shows that the $f_{\text{gas}} = 0.8$ dwarf galaxies reach their first pericenter, thus in the absence of any tidal shocks, already with reduced total central mass. Such a decrease is due to rapid gas outflows at sub-kiloparsec scales, driven by multiple SN explosions, which induce strong and repeated fluctuations in the dwarf gravitational potential. Such fluctuations result in energy transfer to the collisionless components (DM and stars), significantly lowering the total central densities of dwarf galaxies (e.g., Governato et al. 2010; Pontzen & Governato 2012; Teyssier et al. 2013;

Shen et al. 2014; Oñorbe et al. 2015; Read et al. 2016). Due to the increased SF, the overall effect of SN winds is expected to be stronger for higher gas fractions. In conjunction with the impact of ram pressure, this naturally explains the trend of augmented transformation efficiency with larger f_{gas} .

5. DISCUSSION

The present study is the first to elucidate the combined effects of radiative cooling, ram-pressure stripping, SF (based on a high gas density threshold), SN feedback, and a cosmic UV background on the tidal stirring mechanism for the origin of dSphs. We have shown that, regardless of orbit inside the primary galaxy, gas-rich ($f_{\text{gas}} \gtrsim 0.5$) rotationally supported dwarfs exhibit a substantially enhanced likelihood and efficiency of transformation into dSphs relative to their collisionless ($f_{\text{gas}} = 0$) counterparts (Columns 711; Table 3). Such large values of f_{gas} are akin to those of observed dIrrs (e.g., McConnachie 2012; Oh et al. 2015), suggesting that the morphology-density relation (e.g., Mateo 1998), an essential constraint that any theoretical model for the LG must satisfy, may naturally arise in the context of the tidal stirring model.

We gauged the effect of ram pressure on our results by repeating simulation S8 without the hot gas halo in the host. In the absence of ram pressure, the gas was not entirely stripped from the dwarf ($\sim 40\%$ of the original gas content still remained bound). With the obvious caveat that we only explored a single orbit, this experiment suggests that ram pressure is required for the formation of bona fide dSphs via the tidal stirring of gas-rich rotationally supported dwarfs. Our finding that gravitational tides alone, although aided by SN feedback in our case,

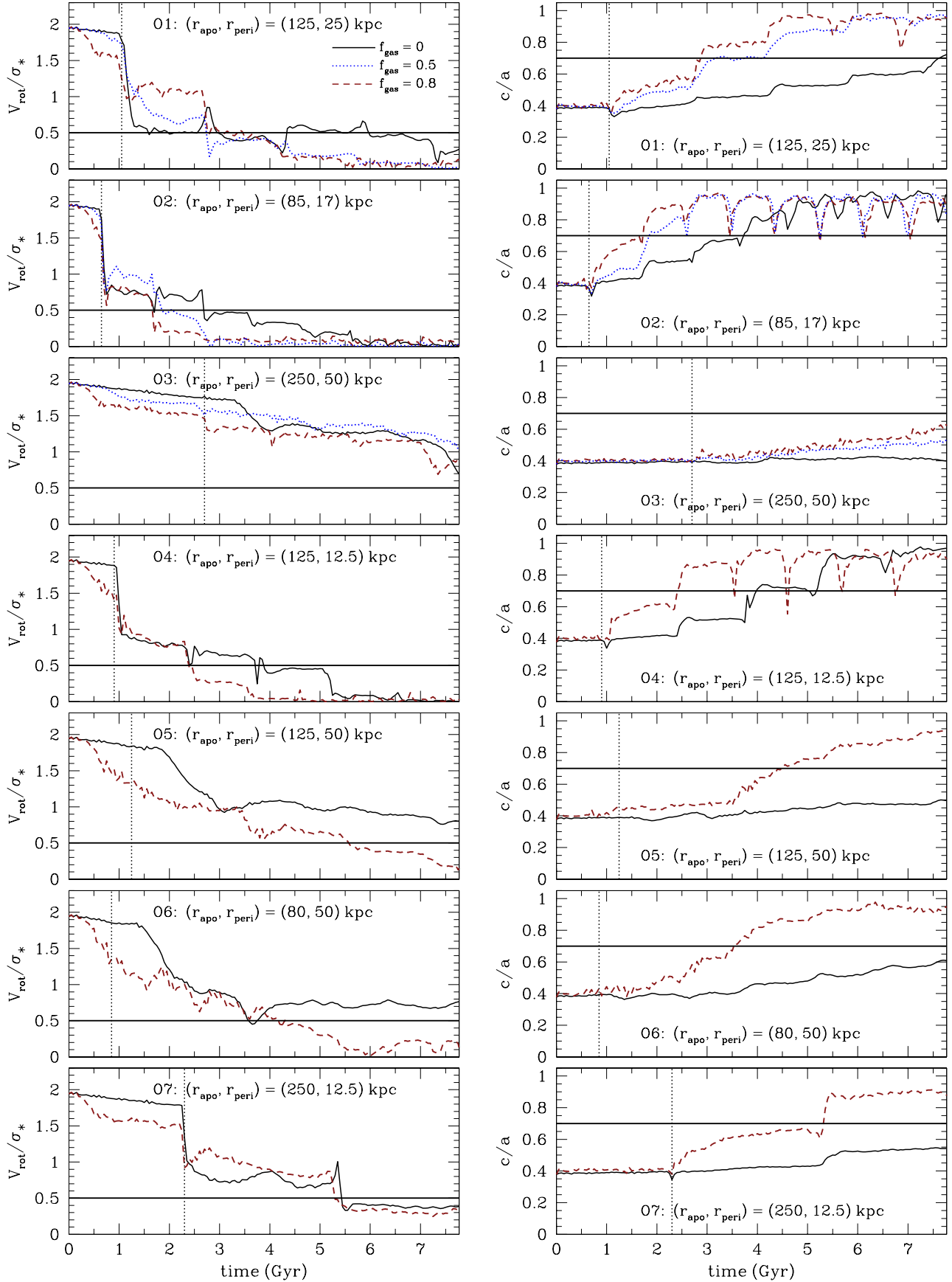


FIG. 1.— Evolution of the stellar kinematics (left panels) and shapes (right panels) of the simulated disk galaxies as a function of time. The results are presented for orbits O1–O7. f_{gas} denotes the fraction of the disk mass in gas and the solid, dashed, and dotted lines correspond to $f_{\text{gas}} = 0$, $f_{\text{gas}} = 0.5$, and $f_{\text{gas}} = 0.8$, respectively. In each panel, the vertical line specifies the initial pericentric passage. The horizontal lines indicate the limiting values $V_{\text{rot}}/\sigma_* = 0.5$, and $c/a = 0.7$: simulated dwarf galaxies whose final states are characterized by $V_{\text{rot}}/\sigma_* \lesssim 0.5$, $c/a \gtrsim 0.7$, and $M_{\text{gas}} \simeq 0$ correspond to bona fide dSphs. For a given orbit, gas-rich ($f_{\text{gas}} \gtrsim 0.5$) rotationally supported dwarfs experience a stronger evolution in their shapes and kinematics and exhibit a considerably enhanced likelihood and efficiency of transformation into dSph-like systems relative to their collisionless ($f_{\text{gas}} = 0$) counterparts.

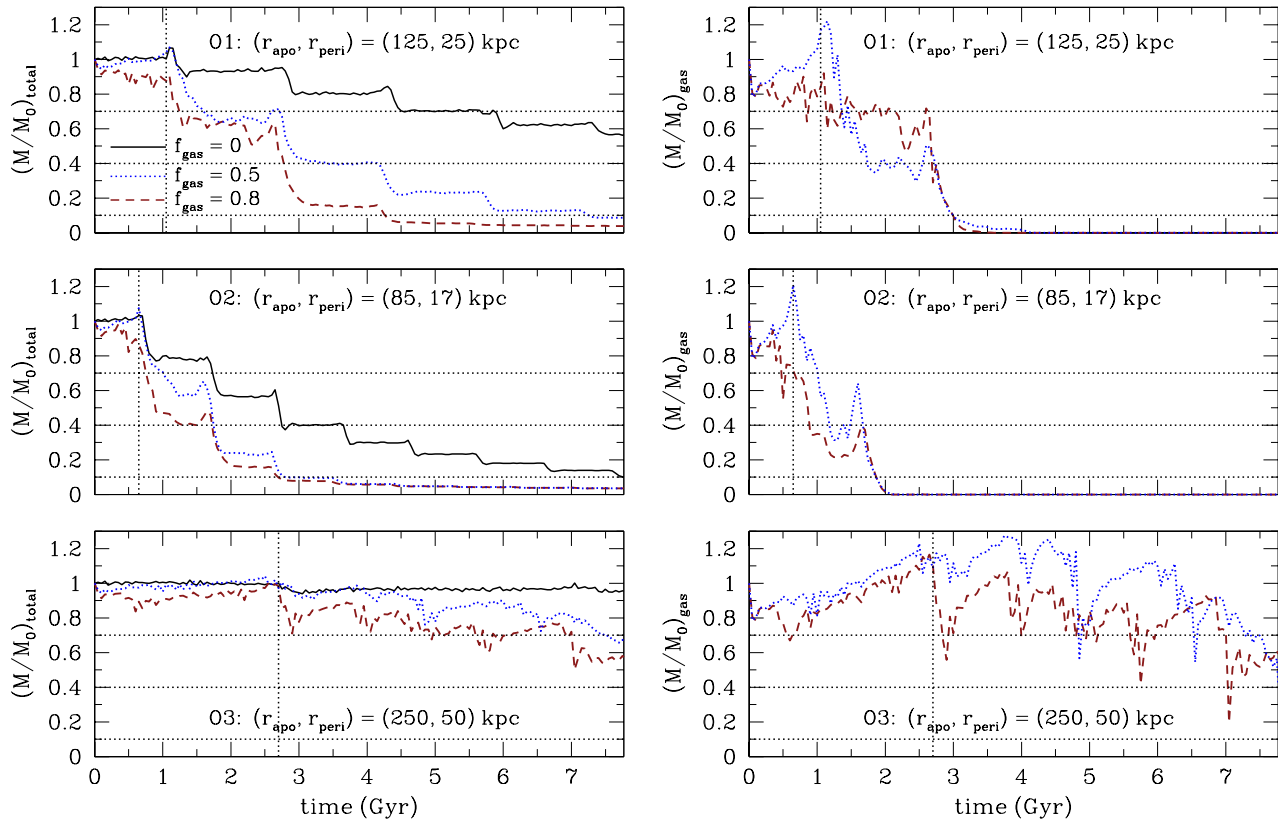


FIG. 2.— Evolution of total (left panels) and gas (right panels) mass of the simulated disk dwarf galaxies as a function of time. The results are presented for orbits O1 (upper panels), O2 (middle panels), and O3 (lower panels). Line types are as in Figure 1. Total (gas) masses are computed within 0.76 kpc from the center of the dwarf (see the text for details) and are normalized to the initial total (gas) mass enclosed within 0.76 kpc, M_0 . In all panels, horizontal lines indicate mass loss of 30%, 60%, and 90% with respect to M_0 . For a given orbit, gas-rich ($f_{\text{gas}} \gtrsim 0.5$) rotationally supported dwarfs suffer enhanced mass loss compared to their collisionless ($f_{\text{gas}} = 0$) counterparts.

cannot entirely remove the gas components from dwarfs, is in agreement with Mayer et al. (2006).

In addition, we ascertained how the transformation process depends on SN feedback by resimulating experiment S8 without this effect. The absence of SN explosions resulted in a notably decreased efficiency of dSph formation, with the timescales of ram-pressure stripping becoming significantly longer (see, also, Mayer et al. 2006). Specifically, complete gas removal now takes place at 5.85 Gyr (and after four pericentric passages), compared to 3.55 Gyr (and after two pericentric passages) in the original simulation S8. This highlights the vital role of SN winds in enabling rapid ram-pressure stripping by making cold gas more loosely bound and by carving holes in the ISM with expanding bubbles that increase ablation effects (e.g., Murakami & Babul 1999; Marcolini et al. 2004).

Although the exclusion of SN feedback did not affect the overall likelihood of transformation, as a bona fide dSph still formed, it did influence the degree of transformation. Indeed, the final values of V_{rot}/σ_* and c/a were equal to 0.25 and 0.81, respectively (compared to $V_{\text{rot}}/\sigma_* = 0.12$ and $c/a = 0.95$, when SN feedback was included; see Table 3). As discussed in Section 4, the less complete transformation in this case is attributed to both the less efficient ram-pressure stripping and the absence of gas outflows from SN winds, causing a more adiabatic response of the disk dwarfs to tidal effects.

Previous work on tidal stirring that did not include SN explosions indicated that the timescales of ram-pressure stripping, and consequently those of dSph formation, were sensitive to the presence of a cosmic ionizing background (e.g., Mayer et al. 2006). We examined this assertion by repeating simulation S8 without the cosmic UV and found that its absence had virtually no effect on either the timescales of ram-pressure stripping or on the efficiency, likelihood, and degree of transformation. Similar conclusions were reached in the experiments with a stronger cosmic UV background (S18–S20; Table 3). These results again underscore the fundamental importance of SN feedback as the primary heating mechanism for the gas and the main effect that facilitates ram-pressure stripping.

We also investigated whether the alignment between the internal and orbital angular momentum of the dwarfs can affect their transformation. To this end, we repeated simulations S1 and S8, adopting a *mildly* retrograde alignment of $i = -45^\circ$. The analysis of these experiments showed that the collisionless disk dwarf does not transform into a dSph (see, also, Lokas et al. 2015), highlighting the importance of coupling between orbital and internal motions; however, its gas-rich counterpart does experience transformation, although with significantly decreased efficiency ($t_{\text{dSph}} = 6.1$ Gyr, as opposed to $t_{\text{dSph}} = 3.55$ Gyr in the prograde simulation; Table 3). In addition, the ram-pressure stripping timescales were

longer and the degree of transformation was substantially weaker in the retrograde case. Mildly retrograde alignments thus seem to support the general picture presented in this study.

Earlier tidal stirring studies established a strong association between the development of long-lived bars in the disks of the progenitor disk dwarfs and dSph formation (e.g., Mayer et al. 2001b,a; Klimentowski et al. 2009; Kazantzidis et al. 2011, 2013). Nonetheless, with the prominent exception of the LMC, the number of irrefutable bar-like distortions observed in LG dwarfs is extremely low (see, however, Lokas et al. 2012), challenging the overall predictive power of the tidal stirring model.

Interestingly, our results indicate that bar formation is not a *necessary* condition for the transformation of rotationally supported gas-rich dwarfs via tidal stirring (Column 6; Table 3), alleviating the tension between observations and theoretical predictions. In these cases, the lower stellar mass fractions, which correspond to a lower self gravity of the tidally perturbed stellar disk, prevent the development of a bar, and dSph-like systems are produced only via tidal heating.

Lastly, our findings demonstrate a correlation between the amount of residual gas in the dwarfs and their degree of transformation into dSphs (Table 3). Specifically, total gas stripping is required for the most complete transformations, while the presence of gas is associated with objects that maintain, at least partially,

the properties of their disk progenitors (S10, S17, S20). The latter finding is particularly relevant to the “transition-type” dwarfs (e.g., Phoenix, Pegasus, and LGS3), which share properties with both dSphs and dIRrs (Grcevich & Putman 2009). One possibility for their origin is that their progenitors were disk satellites that were only recently accreted by their hosts on very wide, radial orbits. These transition-type dwarfs could therefore still be in the process of being transformed into dSphs by tidal stirring, having concluded one pericentric passage and having some of their gas removed via ram pressure. In fact, ram-pressure stripping has been proposed to explain the presence of H_I clouds in the vicinity of Phoenix (Gallart et al. 2001). In the aforementioned scenario, transition-type dwarfs should possess appreciable stellar rotation, having been only partially transformed. Although recent studies have reported significant rotation in both Pegasus (Wheeler et al. 2017) and Phoenix (Kacharov et al. 2017) with $V_{\text{rot}}/\sigma_* \approx 1$, irrefutable evidence of substantial rotation in these systems would be required to validate our prediction.

We acknowledge stimulating discussions with Thanos Anastopoulos, Giuseppina Battaglia, and David Weinberg. S.K. was supported by the Pauli Center for Theoretical Studies at the University of Zürich during the final stages of this work. The numerical simulations were performed at JPL.

REFERENCES

- Abadi, M. G., Moore, B., & Bower, R. G. 1999, MNRAS, 308, 947
 Arraki, K. S., Klypin, A., More, S., & Trujillo-Gomez, S. 2014, MNRAS, 438, 1466
 Assmann, P., Fellhauer, M., Wilkinson, M. I., Smith, R., & Blańa, M. 2013, MNRAS, 435, 2391
 Bate, M. R. & Burkert, A. 1997, MNRAS, 288, 1060
 Diemand, J., Kuhlen, M., & Madau, P. 2007, ApJ, 667, 859
 D’Onghia, E., Besla, G., Cox, T. J., & Hernquist, L. 2009, Nature, 460, 605
 Dotti, M., Colpi, M., Haardt, F., & Mayer, L. 2007, MNRAS, 379, 956
 Einasto, J., Saar, E., Kaasik, A., & Chernin, A. D. 1974, Nature, 252, 111
 Faber, S. M. & Lin, D. N. C. 1983, ApJL, 266, L17
 Gallart, C., Martínez-Delgado, D., Gómez-Flechoso, M. A., & Mateo, M. 2001, AJ, 121, 2572
 Gnedin, O. Y. & Ostriker, J. P. 1999, ApJ, 513, 626
 Governato, F., Brook, C., Mayer, L. et al. 2010, Nature, 463, 203
 Grcevich, J. & Putman, M. E. 2009, ApJ, 696, 385
 Haardt, F. & Madau, P. 2012, ApJ, 746, 125
 Kacharov, N., Battaglia, G., Rejkuba, M. et al. 2017, MNRAS, 466, 2006
 Kazantzidis, S., Lokas, E. L., Callegari, S., Mayer, L., & Moustakas, L. A. 2011, ApJ, 726, 98
 Kazantzidis, S., Lokas, E. L., & Mayer, L. 2013, ApJL, 764, L29
 Klimentowski, J., Lokas, E. L., Kazantzidis, S., Mayer, L., & Mamon, G. A. 2009, MNRAS, 397, 2015
 Klimentowski, J., Lokas, E. L., Knebe, A., Gottlöber, S., Martínez-Vaquero, L. A., Yepes, G., & Hoffman, Y. 2010, MNRAS, 402, 1899
 Kravtsov, A. V., Gnedin, O. Y., & Klypin, A. A. 2004, ApJ, 609, 482
 Kroupa, P. 1997, New Astronomy, 2, 139
 Lokas, E. L., Majewski, S. R., Kazantzidis, S., Mayer, L., Carlin, J. L., Nidever, D. L., & Moustakas, L. A. 2012, ApJ, 751, 61
 Lokas, E. L., Semczuk, M., Gajda, G., & D’Onghia, E. 2015, ApJ, 810, 100
 Macciò, A. V., Dutton, A. A., van den Bosch, F. C., Moore, B., Potter, D., & Stadel, J. 2007, MNRAS, 378, 55
 Marcolini, A., Brighenti, F., & D’Ercole, A. 2004, MNRAS, 352, 363
 Mashchenko, S., Couchman, H. M. P., & Wadsley, J. 2006, Nature, 442, 539
 Mastropietro, C., Moore, B., Mayer, L., Wadsley, J., & Stadel, J. 2005, MNRAS, 363, 509
 Mateo, M. L. 1998, ARA&A, 36, 435
 Mayer, L., Kazantzidis, S., Mastropietro, C., & Wadsley, J. 2007, Nature, 445, 738
 Mayer, L., Mastropietro, C., Wadsley, J., Stadel, J., & Moore, B. 2006, MNRAS, 369, 1021
 Mayer, L., Governato, F., Colpi, M. et al. 2001a, ApJ, 55 9, 754
 Mayer, L., Governato, F., Colpi, M. et al. 2001b, ApJL, 5 47, L123
 McConnachie, A. W. 2012, AJ, 144, 4
 Miller, M. J. & Bregman, J. N. 2013, ApJ, 770, 118
 Mo, H. J., Mao, S., & White, S. D. M. 1998, MNRAS, 295, 319
 Murakami, I. & Babul, A. 1999, MNRAS, 309, 161
 Navarro, J. F., Eke, V. R., & Frenk, C. S. 1996a, MNRAS, 283, L72
 Navarro, J. F., Frenk, C. S., & White, S. D. M. 1996b, ApJ, 462, 563
 Oñorbe, J., Boylan-Kolchin, M., Bullock, J. S. et al. 2015, MNRAS, 454, 2092
 Oh, S.-H., Hunter, D. A., Brinks, E. et al. 2015, AJ, 149, 180
 Pawłowski, M. S., Kroupa, P., & de Boer, K. S. 2011, A&A, 532, A118
 Pontzen, A. & Governato, F. 2012, MNRAS, 421, 3464
 Read, J. I., Agertz, O., & Collins, M. L. M. 2016, MNRAS, 459, 2573
 Read, J. I. & Gilmore, G. 2005, MNRAS, 356, 107
 Read, J. I., Wilkinson, M. I., Evans, N. W., Gilmore, G., & Klypin, J. T. 2006, MNRAS, 366, 429
 Sawala, T., Scannapieco, C., Maio, U., & White, S. 2010, MNRAS, 402, 1 599
 Shen, S., Madau, P., Conroy, C., Governato, F., & Mayer, L. 2014, ApJ, 792, 99
 Skillman, E. D., Monelli, M., Weisz, D. R. et al. 2017, ApJ, 837, 102

- Stinson, G., Seth, A., Katz, N., Wadsley, J., Governato, F., & Quinn, T. 2006, *MNRAS*, 373, 1074
- Teyssier, R., Pontzen, A., Dubois, Y., & Read, J. I. 2013, *MNRAS*, 429, 3068
- Tomozeiu, M., Mayer, L., & Quinn, T. 2016, *ApJ*, 818, 193
- Wadsley, J. W., Stadel, J., & Quinn, T. 2004, *New Astronomy*, 9, 137
- Wheeler, C., Pace, A. B., Bullock, J. S. et al. 2017, *MNRAS*, 465, 2420
- Widrow, L. M., Pym, B., & Dubinski, J. 2008, *ApJ*, 679, 1239
- Yozin, C. & Bekki, K. 2012, *ApJL*, 756, L18